Diffusion Monte Carlo Study of Para - Diiodobenzene Polymorphism Revisited

Diffusion Monte Carlo Study of *Para*-Diiodobenzene Polymorphism Revisited

Kenta Hongo,[*,†] Mark A. Watson,[‡] Toshiaki Iitaka,[¶] Alán Aspuru-Guzik,[§] and Ryo Maezono[†]

School of Information Science, JAIST, Asahidai 1-1, Nomi, Ishikawa 923-1292, Japan, Department of Chemistry, Princeton University, Princeton NJ 08540, Computational Astrophysics Laboratory, RIKEN, 2-1 Hirosawa, Wako, Saitama, 351-0198, Japan, and Department of Chemistry and Chemical Biology, Harvard University, Cambridge, Massachusetts 02138

E-mail: kenta_hongo@mac.com

[*]To whom correspondence should be addressed
[†]School of Information Science, JAIST, Asahidai 1-1, Nomi, Ishikawa 923-1292, Japan
[‡]Department of Chemistry, Princeton University, Princeton NJ 08540
[¶]Computational Astrophysics Laboratory, RIKEN, 2-1 Hirosawa, Wako, Saitama, 351-0198, Japan
[§]Department of Chemistry and Chemical Biology, Harvard University, Cambridge, Massachusetts 02138

Abstract

We revisit our investigation of the diffusion Monte Carlo (DMC) simulation of *p*-DIB molecular crystal polymorphism. [J. Phys. Chem. Lett. 2010, 1, 1789-1794] We perform, for the first time, a rigorous study of finite-size effects and choice of nodal surface on the prediction of polymorph stability in molecular crystals using fixed-node DMC. Our calculations are the largest which are currently feasible using the resources of the K computer and provide insights into the formidable challenge of predicting such properties from first principles. In particular, we show that finite-size effects can influence the trial nodal surface of a small $(1\times1\times1)$ simulation cell considerably. We therefore repeated our DMC simulations with a $1\times3\times3$ simulation cell, which is the largest such calculation to date. We used a DFT nodal surface generated with the PBE functional and we accumulated statistical samples with $\sim 6.4\times10^5$ core-hours for each polymorph. Our final results predict a polymorph stability consistent with experiment, but indicate that results in our previous paper were somewhat fortuitous. We analyze the finite-size errors using model periodic Coulomb (MPC) interactions and kinetic energy corrections, according to the CCMH scheme of Chiesa, Ceperley, Martin, and Holzmann. We investigate the dependence of the finite-size errors on different aspect ratios of the simulation cell (**k**-mesh convergence) in order to understand how to choose an appropriate ratio for the DMC calculations. Even in the most expensive simulations currently possible, we show that the finite size errors in the DMC total energies are far larger than the energy difference between the two polymorphs, although error cancellation means that the polymorph prediction is accurate. Finally, we found that the T-move scheme is essential for these massive DMC simulations in order to circumvent population explosions and large time-step biases.

KEYWORDS: Quantum Chemistry, Diffusion Monte Carlo, Finite Size Errors, Molecular Crystals, Polymorphism

Introduction

The prediction of molecular crystal polymorphism[1,2] is one of the most challenging issues for current *ab initio* electronic structure calculations in both a theoretical and computational sense.[3–23,23–32] The polymorphism is governed by very subtle interactions, such as weak noncovalent bonds. In order to address the problem satisfactorily, theoretical methods must possess sufficient accuracy to reproduce such interactions. In addition, molecular crystals generally have larger and more highly anisotropic unit cells with many more atoms than typical metals or semiconductors. The smallest isotropic simulation cell of the molecular crystal is then larger than that of the uniform crystals, leading to difficulty with the theoretical and computational treatment of such periodic systems. Methods are therefore needed which can strike an appropriate balance between accuracy and computational cost if reliable predictions are to be made.

From the viewpoint of computability, density functional theory (DFT)[33–35] approaches could be candidates for tackling the polymorphism issue. It is well-known, however, that DFT with standard functionals frequently fail to accurately describe noncovalent interactions, especially dispersion.[35] Though many dispersion-related DFT methods[4,36–45] have been exploited and successfully applied recently to typical noncovalent systems,[46] it has been shown that the predictive power strongly depends on the target system. That is, a DFT functional which works well for some specific noncovalent system does not necessarily give good results in another.[47] On the other hand, from the viewpoint of accuracy, post-Hartree-Fock (post-HF) methods such as MP2 (second-order Møller-Plesset perturbation theory) and CCSD(T) (coupled-cluster with single and double excitations including noniterative triples) work well for noncovalent molecular systems. Though the post-HF methods have recently been extended to periodic systems, their computational costs are still too expensive to treat molecular crystals with larger unit cells, and the required additional approximations may weaken their advantage. Very recently, fragment-based schemes have been developed to treat periodic systems in combination with the post-HF methods such as

MP2 and CCSD(T).[3,5,13,14,20] Since their applications to the molecular crystals are limited to typical systems such as water and benzene molecular crystals, more benchmarks would be necessary for assessing their performance in the near future.

It has widely been recognized that quantum Monte Carlo (QMC) methods[48–50] can reproduce various types of molecular interactions to a high accuracy.[47,51–54] Modern massively parallel computers have expanded the applicability of QMC methods not only to larger molecular systems but also to periodic systems because of their high parallel efficiency.[55,56] One of the most practical QMC methods, fixed-node diffusion Monte Carlo (FN-DMC), has been applied to noncovalent molecular systems and demonstrated to have an accuracy comparable to CCSD(T).[47,51–54] Since the accuracy of FN-DMC depends critically on the choice of trial nodal surface, one should take care when generating this surface. If one uses DFT, experience shows that the nodal structures generally depend on the functional employed, and many choices are available in the literature. Although a number of QMC studies have reported that the dependence is not strong, some will be better than others and it is nontrivial to decide which method is best a priori. In spite of this issue, FN-DMC is expected to be applicable to periodic systems with high accuracy in practice. Compared to FN-DMC, the "gold-standard" CCSD(T) method has heavier computational costs, and is unable to typically treat such systems without additional approximations.

When applying QMC methods to periodic systems, one should ideally vary the simulation cell size and extrapolate the results to infinity. But such a full extrapolation in QMC is much more difficult than in DFT even using cutting-edge supercomputers. Therefore tractable simulation cell sizes are quite limited in practice, leading to potentially significant finite-size errors (FSEs) in QMC results. A number of correction schemes have been devised to reduce the effects arising from FSEs. These schemes are formally classified into either one- or two-body types.[57] The one-body schemes for metallic systems differ from those for insulating systems due to the existence/nonexistance of a Fermi surface. The twist-averaging technique due to Lin, Zong, and Ceperley[58] significantly improves the FSEs for metals. The k-point

shift (from Γ to L), similar to the "special k-point method" in DFT, frequently works well for insulators.[59,60] The MPC (model periodic Coulomb interaction)[61,62] and CCMH (Chiesa, Ceperley, Martin, and Holzmann)[63] schemes are known to be effective two-body schemes. In addition, Kwee, Zang, and Krakauer devised an *a posteriori* finite-size correction to the exchange-correlation (XC) potentials within the DFT framework (KZK scheme).[64] The KZK scheme has been recently extended to magnetic systems.[65]

A number of large-scale periodic QMC simulations have been performed.[66–70] They show that the above-mentioned schemes work well for isotropic (mostly cubic) systems having small unit cells with only one or two elements. QMC applications to molecular crystals have been traditionally restricted to relatively simple systems, e.g., phase diagrams of ice[71] and sold molecular hydrogen.[72] It has generally been unfeasible to simulate more strongly anisotropic and complicated molecular crystals because of the limits imposed by available computational resources (mostly memory size). In our previous study,[73,74] we investigated for the first time using FN-DMC the polymorphism of the para-diiodobenzene (p-DIB) organic molecular crystal, a strongly anisotropic system. Standard DFT methods contradict experiment in that they predict the α phase to be more stable than the β phase at zero temperature. Our FN-DMC results were consistent with experiment, but they were only performed using an LDA nodal surface and a small $1 \times 1 \times 1$ simulation cell. Since they were the largest calculations we could do at that time using the available supercomputer resources, we adopted the empirical KZK scheme[64] to estimate the FSEs. Very recently, more sophisticated DFT simulations were performed based on DFT-Δ_{12}[12] and DFT-D,[10] both of which agreed with our FN-DMC results. This does not imply, however, that the KZK scheme adopted in our previous study appropriately describes the FSEs in our FN-DMC simulations because there is no *a priori* reason that the FSEs in isotropic systems should be similar to those in anisotropic systems. In this sense, our previous study had some limitations, and it is not clear how large the FSEs were, or whether the above-mentioned schemes can effectively correct them for anisotropic molecular crystals. Thus, the following

two points should be carefully investigated in the FN-DMC simulations of the *p*-DIB molecular crystal polymorphism: (1) FSE effects for anisotropic molecular crystals, *i.e.*, choice of simulation cell size, their aspect ratios and the performance of finite-size correction schemes; (2) the nodal surface dependence for an accurate description of noncovalent interactions.

We shall report here that our previous FN-DMC result (DMC/LDA/$1\times1\times1$) appears to be fortuitously accurate. In the present study, we show that FN-DMC simulations of the polymorph stabilities with a $1\times1\times1$ unit cell show quite a strong dependence on the choice of nodal surface: e.g. LDA, GGA-PBE, or B3LYP. In particular, we found early on that the DMC/PBE/$1\times1\times1$ result contradicts experiment by predicting the β phase to be most stable, in contrast to our previous paper using an LDA surface. This encouraged us to carefully investigate the results with different nodal surfaces and compare them. We therefore also investigated how the sizes and aspect ratios of simulation cells affect the FSEs within DFT. When taking any two sufficiently large cells, we confirmed that extrapolation of the two energies converges to the same final energy regardless of the cells' aspect ratios. However, when using smaller cell sizes with three different aspect ratios, 1×1, 1×2, and 1×3, we observed significantly different final energies after extrapolation. This implies that the choice of aspect ratio is especially significant for QMC because it is only applicable to smaller unit cell sizes. In this work, we have performed the largest possible DMC/PBE simulations given our available computational resources on the K computer,[75] with an approximately isotropic $1\times3\times3$ simulation cell. We found that the correct prediction is recovered when we increase the simulation size from $1\times1\times1$ to $1\times3\times3$, implying significant finite size effects in this system. Even with a $1\times3\times3$ cell, the FSE schemes we used (MPC/CCMH) are found to give corrections far larger than the energy difference between the polymorphs. Hence further detailed investigation of finite size errors is necessary for the definitive resolution of these questions in such anisotropic systems, which are often intriguing materials such as strongly-correlated electron systems and molecular crystals.

The paper is organized as follows: Section "Computational Methods" specifies our target

systems and methodologies. Section "Results" simply deals with our numerical results of relative stability energies obtained from QMC. Section "Discussions" gives a detailed analysis of several finite-size corrections as well as computational aspects in our DMC simulations.

Computational Methods

Target Systems

We treated two polymorphs of the *para*-diiodobenzene (*p*-DIB) molecular crystal, known as the α and β phases. The transition from α to β occurs at 327K indicating that the α phase is slightly more stable than the β phase at low temperature.[76,77] To the best of our knowledge, the relative energy between the two phases at zero temperature is not available from any experiment. The lattice symmetries for the α and β polymorphs belong to the *Pbca* (D_{2h}^{15}) and *Pccn* (D_{2h}^{10}) space groups, respectively, but they both have four *p*-DIB molecules in an orthorhombic unit cell (see Fig. 1). All the present calculations were performed using experimental molecular geometries (lattice constants and unit cell atomic positions) published in the Cambridge Structural Database[78] (ZZZPRO03 and ZZZPRO04 for the α and β phases, respectively). Note that the unit cell for each phase has an aspect ratio of almost 3×1, indicating strong anisotropy.

Methods

For general descriptions of QMC methods adopted in the present study there are several recent review articles[48–50] available. To investigate the FSEs in the DMC calculations of *p*-DIB, we consider the $1 \times 1 \times 1$ and $1 \times 3 \times 3$ simulation cells. Although the k-mesh size convergence in DFT does not coincide with the one-body FSE in DMC completely, it is helpful to understand how the one-body FSE decreases, depending the aspect ratio, as the size increases. To see this, we considered $1 \times 1 \times 1$, $1 \times 2 \times 2$, $1 \times 3 \times 3$, $2 \times 4 \times 4$, and $2 \times 6 \times 6$ Monkhorst-Pack $\mathbf{k}$-point mesh sizes.[79] We performed LDA (Perdew-Zunger 81; PZ81[80]) and

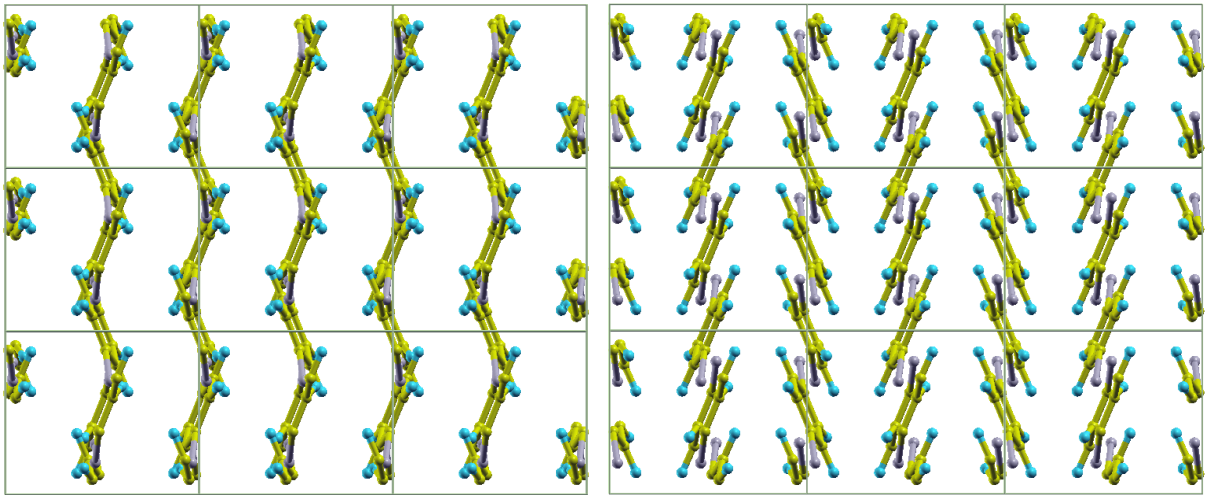

Figure 1: The $1\times3\times3$ simulation cells of the α (left) and the β (right) phases with orthorhombic symmetry, viewed along the a-axis (bc-plane). The α phase has a unit cell with lattice constants $a = 17.000$, $b = 7.323$, and $c = 6.168$ Å, while β has $a = 17.092$, $b = 7.461$, and $c = 6.154$ Å. Pictures are scaled so that both phases have the same size in the b-axis direction.

GGA (Perdew-Burke-Ernzerhof; PBE[81]) calculations. In addition, we attempted to get results with the B3LYP functional,[82–84] but unfortunately they did not converge, except in the $1\times1\times1$ case. All the DFT calculations were performed using the `Quantum Espresso` code.[85] The crystalline orbitals were expanded in a plane-wave basis set with a cutoff energy of 40 hartree, such that the energy differences between the two polymorphs converged to 0.01 kcal/mol/cell. The ionic cores of the carbon, iodine, and hydrogen atoms were replaced by Trail-Needs pseudopotentials (TN-PPs),[86,87] available in the CASINO pseudopotential library.[88] Note that the TN-PPs were developed for QMC, but can also be used for plane-wave based DFT calculations.

For the DMC simulations, we adopted Slater-Jastrow type wavefunctions as trial fixed-nodes.[48–50] We considered DMC/LDA/1×1×1, DMC/GGA/1×1×1, DMC/B3LYP/1×1×1, and DMC/GGA/1×3×3, where "DMC/DFT/$1\times n\times n$" represents a DMC simulation with the DFT node using $1\times n\times n$ cell size ($n = 1$ or 3). In our previous study, we used `QMCPACK`[89] for the DMC calculations with LDA[90] fixed nodes obtained by `ABINIT`.[91,92] In the present study, we instead used the `CASINO` code[48] to see how the MPC interaction[61,62] and T-move

scheme[93] implemented therein work. The KZK finite-size correction[64] is available in the `Quantum Espresso` code[85] and we applied it to the present DMC/LDA/$1\times1\times1$ case. To speed up the QMC calculations, we transformed the plane wave orbitals into a blip basis.[94] For the trial wavefunctions, we took a form of Jastrow functions[95] implemented in `CASINO`,[96] consisting of one-body and two-body terms (imposing the cusp conditions[97]). The former has 24 adjustable parameters with a cutoff length fixed at 80% of the Wigner-Seitz radius of the simulation cell, while the latter has 12 parameters with a cutoff equal to the Wigner-Seitz radius. All the parameters that appeared linearly in the Jastrow function were optimized by minimization schemes. For handling tiny energy differences such as those in molecular crystal polymorphs, it would be more appropriate to adopt the minimization of the mix of energy and variance[98] in general. In the present study, however, we limited ourselves to optimize the linear parameters with non-linear ones fixed (e.g., cutoff lengths), using the variance minimization technique.[99] This gives a unique minimum with much lower cost.

We employed our 32-core PC clusters to run the DMC simulations for the $1\times1\times1$ cell size. Since the $1\times3\times3$ cell size simulations require approximately 729 ($=9^3$) times greater computational cost, we used the K computer[75] with 1,024-node (2,048-core) parallelization. The simulation for each polymorph took about 5×10^5 core-hours. We evaluated the electron-electron interaction using both the Ewald[100,101] and MPC[61,62] schemes, but only the Ewald energy was used in the DMC propagation because it is known that the MPC may artificially distort the exchange-correlation hole in some cases.[57] We set the target DMC population numbers ($N_{\rm pop}$) to be 1,280 and 20,480 for the $1\times1\times1$ and $1\times3\times3$ cell size calculations, respectively. The T-move scheme[93] was used to evaluate the pseudopotentials with the locality approximation so that the bias can be reduced and to allow the population control[102] be more stable. After equilibrating the random walkers over the first 1,500 steps, we accumulated statistics over the following 1×10^5 and 7×10^3 steps ($N_{\rm step}$) for the $1\times1\times1$ and $1\times3\times3$, respectively.

Results

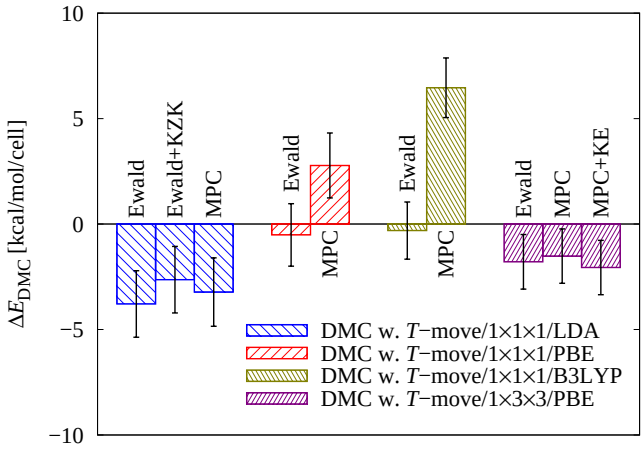

Figure 2: DMC energy differences between α and β polymorphs of p-DIB, $\Delta E_{\rm DMC} = E_{\rm DMC}(\alpha) - E_{\rm DMC}(\beta)$, evaluated at the experimental geometry using Ewald and MPC interactions. All the DMC calculations were performed with the T-move scheme.[93] While LDA, PBE, and B3LYP functionals are used to generate the fixed-node surfaces for the $1\times1\times1$ cell, only PBE is considered for the $1\times3\times3$ cell. The KZK finite-size error correction is considered only for the DMC/LDA/$1\times1\times1$ case (see text). The FSE correction to the kinetic energy calculated using the CCMH scheme is taken into account only for the DMC/PBE/$1\times3\times3$ case (shown as 'KE'). Energies are given in units of kcal/mol per unit cell.

Figure 2 shows the DMC evaluations of the energy difference between the two phases, $\Delta E_{\rm DMC} = E_{\rm DMC}(\alpha) - E_{\rm DMC}(\beta)$. Here we carried out DMC/LDA/1×1×1, DMC/PBE/1×1×1, DMC/B3LYP/$1\times1\times1$, and DMC/PBE/$1\times3\times3$ simulations. The figure also provides a comparison between the results with different interaction schemes, *i.e.*, Ewald and MPC.[61,62] A striking fact is that the stability prediction of the polymorphs with the $1\times1\times1$ cell size strongly depends on the interaction schemes used, showing a severe effect from FSEs. While the DMC/LDA/$1\times1\times1$ results are consistent with DMC/GGA/$1\times3\times3$ and experiment, those with other nodal surfaces (GGA and B3LYP) give an uncertain or wrong prediction of the polymorph stability. Large energy differences between the Ewald and MPC results imply that the simulation size is still too small to adequately remove FSEs.[57] Thus we have to conclude that the $1\times1\times1$ predictions are not reliable in general and that our previous

work[73,74] (DMC/LDA/$1\times1\times1$) gave fortuitously good results.

Both DMC/LDA/$1\times1\times1$ and DMC/PBE/$1\times3\times3$ give the correct sign for $\Delta E_{\rm DMC}$, *i.e.*, consistent with experiment (i.e. the α phase being more stable than the β at zero temperature). They give the same value within the error bars regardless of the correction scheme, typically $\Delta E_{\rm DMC} = -2 \pm 1$ ($1\times3\times3$/Ewald). Finally, we shall see the effect of the KZK finite-size correction.[64] It has been reported that the KZK correction, combined with the LDA finite-size functional, would succeed in correcting the FSE for isotropic systems if the LDA functional could provide a reasonable description of the system considered.[57,64] Although the $1\times1\times1$ cells of *p*-DIB polymorphs are anisotropic, the KZK approach applied to this case is found to work well.

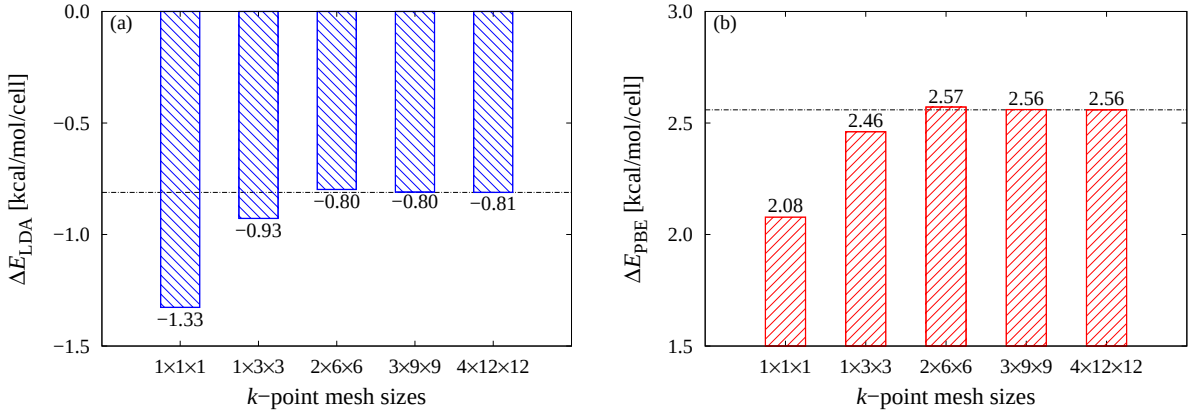

Figure 3: Energy differences between α and β polymorphs of *p*-DIB, $\Delta E = E(\alpha) - E(\beta)$, for (a) LDA and (b) PBE with various k-point mesh sizes. Each energy is given in units of kcal/mol per unit cell.

Discussions

Finite size errors

It has been found in Fig. 2 that there is a significant dependence of the DMC relative energy on the choice of XC functional for $1\times1\times1$ predictions. This suggests that the functional dependence of our DMC/$1\times3\times3$ results should be examined more carefully, even though

PBE gives a successful prediction. Unfortunately, the evaluation is too expensive for our computational resources. We estimate it would require more than a month of CPU time on the K computer using 2,048 cores. Though further investigation of the functional dependence would be an interesting challenge, we shall concentrate on the available results coupled with two approaches to estimate FSEs: (1) extrapolations of the k-mesh dependence within DFT; (2) comparison of the Ewald/MPC and CCMH schemes within QMC/1×3×3. The former and the latter give useful insights about one-body and two-body FSEs, respectively, although they do not completely describe the effects.

Figure 3 compares the DFT/LDA and DFT/PBE results in terms of their mesh-size dependence. The negative ΔE_{LDA} values seen in panel (a) show that these calculations reasonably predict the α phase to be more stable than the β phase. In contrast, DFT/PBE fails to reproduce the correct relative stability even when convergence with respect to mesh size is achieved. This may be intriguing because the PBE trial nodal surface with the 1×3×3 cell size gives the correct prediction ($E[\alpha] < E[\beta]$) when combined with DMC projection. We found that the LDA (PBE) difference in E between 1×3×3 and 4×12×12 is −0.15 (−0.13) and −0.03 (−0.03) kcal/mol/cell for α and β, respectively, and consequently, the difference in ΔE becomes −0.12 (−0.10) kcal/mol/cell. Hence we may expect the 1×3×3 cell size to be large enough to produce QMC trial nodes which may lead to a one-body FSE as small as the corresponding DFT approaches. Even if the nodes gave a large one-body FSE in the QMC total energy for each polymorph, a favorable error cancellation between the two polymorphs would significantly reduce the one-body FSE in the QME energy difference. Here we briefly make a comment on the above-mentioned LDA result. Though LDA cannot intrinsically describe dispersion effects, it fortuitously gives the correct relative stability, as shown in Fig. 3. Similar observations have been reported for various other noncovalent molecular systems.[47,103,104] An incomplete description of exchange in LDA is cancelled out by that of correlation responsible for dispersion.

Figure 4 demonstrates the **k**-mesh size dependence of PBE-DFT total energies for $N_k =$

Table 1: Total energies and their differences between Ewald and MPC interactions ($\delta E = E_{\rm MPC} - E_{\rm Ewald}$) for the α and β phases of p-DIB molecular crystals. Energy deviations from PBE/1×1×1 in Ewald are also listed for the α and β phases ($dE[\alpha/\beta]$). Their error bars are given in parenthesis. The positive sign of δE means that the MPC energy $E_{\rm MPC}$ is higher than the Ewald energy $E_{\rm Ewald}$. All the DMC calculations were performed with the T-move scheme,[93] and their energies are given in units of kcal/mol/cell.

	LDA/1×1×1	PBE/1×1×1	B3LYP/1×1×1	PBE/1×3×3
$E_{\rm Ewald}[\alpha]$	$-148,827(1)$	$-148,823(1)$	$-148,832(1)$	$-148,745(1)$
$E_{\rm Ewald}[\beta]$	$-148,823(1)$	$-148,822(1)$	$-148,832(1)$	$-148,743(1)$
$E_{\rm MPC}[\alpha]$	$-148,750(1)$	$-148,745(1)$	$-148,757(1)$	$-148,734(1)$
$E_{\rm MPC}[\beta]$	$-148,747(1)$	$-148,748(1)$	$-148,764(1)$	$-148,733(1)$
$\delta E[\alpha]$	77(2)	78(2)	75(2)	10(1)
$\delta E[\beta]$	76(2)	74(2)	68(1)	10(1)
$dE[\alpha]$	$-4(2)$	NA	$-9(2)$	$+78(1)$
$dE[\beta]$	$-1(2)$	NA	$-10(1)$	$+79(1)$

$N\times\gamma N\times\gamma N$ simulation cell ($\gamma = 1, 2$ and 3). This is useful for understanding how to choose appropriate aspect ratios of the simulation cell, though the results are obtained at the DFT level. Considering the highly anisotropic molecular crystal structures, the ratios of $\gamma = 2$ and 3 are expected to be proper choices, so that their simulation cells are made approximately cubic. For all the choices of γ, extrapolations by taking large enough N converge to the same energy. In contrast, when using small N, we see that there is a significant dependence of the extrapolated values on the choice of the ratio. It is evident from Fig. 3 that extrapolations ($1/N_k \to 0$) by taking only $N = 1$ and 2 lead to unreasonable values. Extrapolation by taking $N = 2$ and 3 still gives a wrong extrapolated value for $\gamma = 1$, but does reasonable ones for $\gamma = 2$ and 3. The results imply that naive extrapolation procedures are quite unreliable for crystals with such anisotropic unit cells and one has to pay attention to the choice of the aspect ratio. This would be closely related to the fact that we got inconsistent QMC predictions using 1×1×1 and 1×3×3.

Though it is known that MPC cannot completely capture the two-body FSE,[57] it may be used as an "alert indicator" to show that the simulation cell size is not large enough when the difference $\delta E = E_{\rm MPC} - E_{\rm Ewald}$ is remarkably large. Table 1 lists δE in kcal/mol/cell for

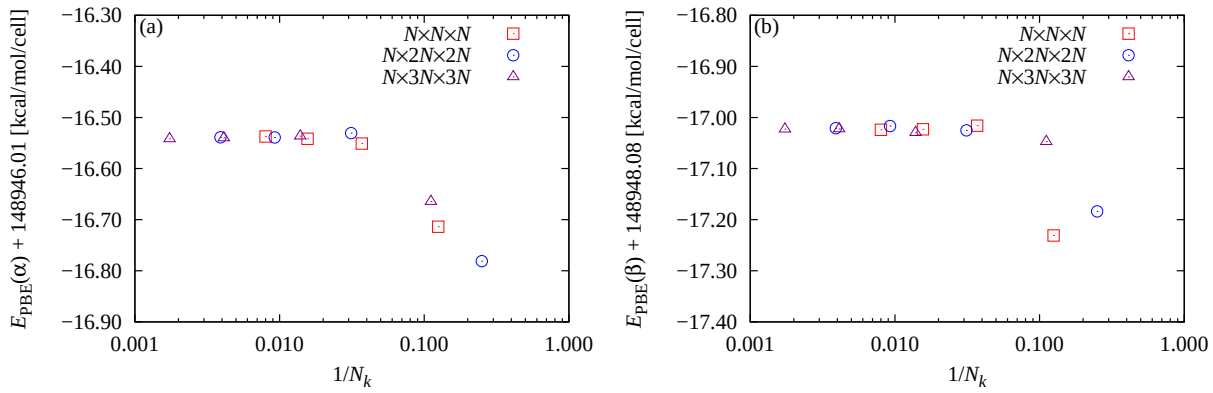

Figure 4: **k**-point mesh dependence of DFT-PBE total energies in units of kcal/mol/cell for (a) the α phase and (b) the β phase. $N_k = N \times \gamma N \times \gamma N$, where $\gamma = 1, 2, 3$. For $\gamma = 1$, N ranges $2 \sim 5$ while for $\gamma = 2 \sim 3$, $N = 1 \sim 4$. Note that the total energies are shifted by their corresponding $1\times1\times1$ values for the two phases, and hence the $1\times1\times1$ results are not shown in these figures.

the α and β phases. The difference in DMC/LDA/$1\times1\times1$ (0.5%) is much larger than that in DMC/PBE/$1\times3\times3$ (0.007%), indicating that $1\times1\times1$ is not large enough, compared with $1\times3\times3$. The positive sign of δE means that the MPC energy is higher than the Ewald energy, which is consistent with well-known facts in the QMC-FSE literature.[57] It is observed that an inequality, $\delta E[\alpha] > \delta E[\beta]$, holds for every DMC simulation, meaning that the FSE is always larger in the α phase. This may be attributed to the larger cell volume of the β phase by $\sim 2.2\%$, compared to the α phase.

The CCMH scheme provides a finite-size correction to the kinetic energy due to the long-ranged correlations described in the two-body Jastrow factor, evaluated from the asymptotic behavior as $k \to 0$. We evaluated the correction using the implementation in CASINO (version 2.11),[48] given as ΔT_2 in Table 2. The corrections for the α and β phases are ca. 5 kcal/mol/cell which amount to a half of the MPC corrections (ca. 10 kcal/mol/cell), indicating that the MPC is insufficient to capture the whole two-body FSE, as mentioned above. The reliability of the correction ΔT_2 can be checked by comparing the estimates obtained from two different asymptotic models.[57] The difference between the two estimates was found to be 3% for α and 11% for β, which seems reasonable. An additional 'p term'

entering the two-body Jastrow factor is found to be indispensable for achieving such accuracy. The p term[48] augments the correct behavior at the simulation cell boundaries by a plane-wave expansion and is important for the quantitative reliability in the correction. Note that a complete lack of the p term gives rise to a difference of 75% and 65% for α and β, respectively.

Table 2: Finite-size corrections in units of kcal/mol/cell for DMC/$1\times3\times3$ with the T-move scheme.[93] Here ΔE_1 indicates the one-body FSE estimated from DFT, ΔT_2 the finite-size corrections to the kinetic energy evaluated by the CCMH scheme, and ΔU_2 the MPC corrections where statistical error bars are in parentheses. ZPE stands for the zero-point vibration energies evaluated by several DFT calculations, where these values were obtained in Ref.[74]

	α	β	$\Delta(\alpha-\beta)$
ΔE_1	0.1	0.0	0.1
ΔT_2	4.4	4.9	-0.5
ΔU_2	10(1)	10(1)	0(2)
ZPE/LDA	198.6	198.4	0.2
ZPE/B3LYP	203.6	203.5	0.1
ZPE/B3LYP+D	206.2	206.2	0.0

Several possible corrections to the DMC/$1\times3\times3$ result are tabulated in Table 2. The largest correction comes from MPC, $\Delta U_2 \approx 10$ kcal/mol/cell, followed by the kinetic correction, $\Delta T_2 \approx 5$ kcal/mol/cell. The $\mathbf{k}$-mesh correction evaluated by DFT, $\Delta E_1 \approx 0.1$ kcal/mol/cell, gives the smallest, which is attributed to the fact that the system is an insulator. We note again that ΔE_1 does not describe the whole one-body FSE in QMC, as mentioned above. Comparing the relative stability of α to β, 2.5 kcal/mol/cell (4 mHa/cell), the FSE corrections themselves ($\sim$ 10 kcal/mol/cell at most) are far larger and hence a careful consideration of FSEs is clearly essential. However, it is reasonable to expect that the corrections would not significantly change the final conclusion that DMC/$1\times3\times3$ can predict the correct stability of α relative to β, because of error cancellation between the two phases ($\Delta(\alpha-\beta)$ in Table 2). We note that we cannot put any quantitative significance on the value, -0.5kcal/mol/cell, of $\Delta(\alpha-\beta)$ in ΔT_2 because of the ambiguity associated with the choice of asymptotic model for the evaluation; i.e. 3% and 11% for the α and β phases,

respectively.

Table 2 also summarizes the zero-point energy (ZPE) effects. We could expect the ZPE difference between the two phases to be negligibly small, because the majority of the ZPE comes from the intramolecular contributions, and the ZPEs are almost the same for the two phases. Actually, the computed ZPE differences evaluated by several DFT methods are less than 0.2 kcal/mol/cell, as shown in our previous study.[74]

For highly anisotropic systems we cannot generally rely on any "handy" FSE correction scheme such as MPC when using a small simulation cell. Instead, we need to attempt a simple extrapolation by enlarging simulation cells with a fixed aspect ratio (approximately cubic). Further QMC investigations using larger simulation cells with various XC functionals would then be required to draw more firm predictions, but they are too expensive to be done. We shall particularly discuss the computational issues in the following subsection.

Computational requirements

In the present study we could not perform $2\times6\times6$ or larger simulations simply because of memory size limitations on the K computer, which has 16GB/node. The $1\times3\times3$ requires 9.8GB/node for storing the wavefunction data (in the blip basis[94]), while a $2\times6\times6$ cell would require 25GB/node. The use of plane-wave basis functions can reduce the capacity required for the wavefunction data from 25 GB/node to 12 GB/node for 2×6×6, but instead the computational time becomes a few hundred times longer. The most recent cutting-edge facilities such as Tianhe-2 (88GB/node) or Titan (34GB/node) might be able to accommodate such calculations. But even with such resources, the larger $2\times6\times6$ cell size seems unfeasible in practice because the cost of the equilibration steps in DMC cannot be reduced by the current parallel implementations. We used a DMC implementation, CASINO, which achieves greater than 99% parallel efficiency even using 6×10^5 cores on the K computer.[105] But it can reduce the cost linearly as the number of cores increases only for the statistical accumulations, not for the preceding equilibration of the sampling distributions. The equili-

bration should be achieved on each parallel core with some required number of steps, which is fixed regardless of the number of cores adopted. When using a tremendous number of cores for large-scale DMC simulations, this implies that the computational cost in terms of cpu-hours is dominated by the equilibration rather than the statistical accumulation.

Table 3 lists the number of cores ($N_{\rm core}$), the number of MC steps ($N_{\rm step}$), computational time (T in hours), computational cost (C in terms of core-hour), and the percentage of the equilibrium cost to the total one (W) in our DMC/1×3×3 simulation on the K computer with 2,048 cores. We also make an estimate for an idealized 512,000-core case, which represents about 70% of the available cores on the K-computer,[75] assuming that the parallel efficiency is 100% and the total number of sampling points in the statistical accumulation (or equivalently, C) is the same for both cases. Because the required cost for the equilibration is the same for each node it increases linearly with the number of cores, going beyond 10 million core-hours when one uses 512,000 cores. It results in a rate of increase in computational cost (R) about 48 times larger to achieve the same speedup (S), about 5 times. Since the QMC computation scales as N^3 with respect to the number of electrons N in the system, the 2×6×6 simulation takes 8 times longer computational time than the 1×3×3 one. This implies that the $2,048$-core parallelization requires 6.2×10^6 core-hours over 128 days, while a theoretical $512,000$-core parallelization requires 3.0×10^8 core-hours over 24 days. They are both too expensive to be done, where the bottleneck lies in the equilibrium computation.

Table 3: The number of cores ($N_{\rm core}$), the number of MC steps ($N_{\rm step}$), computational time (T in hours), computational cost (C in terms of core-hours), and the percentage of the equilibrium cost to the total one (W) are listed for DMC/$1\times3\times3$ simulations with $2,048$- and $512,000$-core. The values for the $512,000$-core parallelization are estimated from those for the $2,048$-core one. A rate of increase in computation cost (R) and speedup (S) from $2,048$ to $512,000$ are also given.

	equilibrium			accumulation					
$N_{\rm core}$	$N_{\rm step}$	T	C	$N_{\rm step}$	T	C	W	R	S
2,048	1,500	72	147,456	6,500	312.000	638,976	18.75	1	1
512,000	1,500	72	36,864,000	26	1.248	638,976	98.34	47.7	5.2

A simple way to speed up the equilibration procedure is to reduce the number of walkers

per core ($N_{\mathrm{w/c}}$), *i.e.*, the computational load on each core. Nevertheless, this is not a good strategy. In the current implementation with the annihilation/creation of walkers, too few $N_{\mathrm{w/c}}$ may lead to the 'dying out of walkers' at several cores, which suspends simulation runs. We can circumvent this difficulty by using the 'weighted walker scheme'[48,106] where the annihilation/creation is replaced by the weight accumulation on a walker. A more pressing reason why we cannot simply reduce N_c, however, arises from a consideration of load-balancing and communication costs.[56] The annihilation/creation occurs individually on each core, bringing about unbalanced loads as a calculation evolves. To recover the balance, inter-node communication redistributes the walkers from populated cores to depopulated ones. However, the time required for the communication (T_{comm}) increases as the number of walkers per core increases ($N_{\mathrm{w/c}}$). On the other hand, the ratio of communication time to CPU time, $T_{\mathrm{comm}}/T_{\mathrm{CPU}}$, decreases as $N_{\mathrm{w/c}}$ increases.[56] Consequently, it is recommended not to reduce $N_{\mathrm{w/c}}$ in order to maintain a high parallel efficiency.

To accelerate the equilibration, computational techniques other than the current MPI parallelization are therefore required. A number of previous QMC studies have demonstrated that hardware accelerators such as graphical processing units (GPU)[107,108] and field-programable gate arrays (FPGAs)[109,110] may be one of the most promising techniques for that purpose. We may hence conclude that naive use of tremendous parallelization is not necessarily a good solution to practical DMC simulations when considering overall cost and performance.

Dependence on Density Functionals

We note that the MPC interaction in DMC/DFT is evaluated using the corresponding DFT charge density. This would introduce a spurious dependence of MPC corrections on XC even in DMC. This may relate to the significant dependence of MPC prediction on XC in DMC/1×1×1 shown in Fig. 2. Applying not large enough simulation cell size (e.g., 1×1×1) to such a strong anisotropic system would lead to improper gradient evaluations in GGA

and hence result in the stronger dependence of MPC on XC due to its poor description of XC holes at DFT level.

By looking only at Ewald/1×1×1 energies, the B3LYP node turns out to give the lowest energy in the variational sense, ca. 10 kcal/mol/cell lower than the other two nodes, shown as dE in Table 1. Though the size 1×1×1 is not reliable for describing the reality of the target system, we can formally evaluate the quality of nodal surfaces upon the 'nodal variational principle'.[111] We note that T-move scheme applied to the present evaluations recovers the principle[93] which is lost under the locality approximation for pseudopotential evaluation.[112] It would be then intriguing to try the same evaluation at 1×3×3 in future if the computational resource is available, even though it is very hard to make DFT/B3LYP/1×3×3 converge. The difference in dE between 1×3×3 and 1×1×1 is due to the FSEs, which almost coincides with δE, namely the estimation of FSE by MPC. This would imply that the MPC estimations work reasonably.

T-move scheme and numerical stability

To perform DMC/$1\times3\times3$ simulations efficiently, we have selected the computational conditions very carefully. Our previous $1\times1\times1$ simulations[73,74] forced us to accumulate an enormous number of steps ($N_{\mathrm{step}} = 1.2\times10^7$) to achieve the required statistical accuracy, even with a large target population ($N_{\mathrm{pop}} = 16,384$). The computation of each phase took about 6 months using 128 cores in those days. In the present study we therefore chose a larger $\delta\tau_{\mathrm{DMC}}$ for a more efficient sampling, which is proved to be possible only with the T-move scheme.[93] This scheme has been devised to suppress a divergence of local energy when a sampling occurs at the nodal surfaces, which is effective to control population explosions in DMC.[93] In the present study, we adopted a CASINO implementation of the T-move scheme.[48] The scheme is found to be essential in this work to complete such a large size simulation with a reasonably small time step bias.

Table 4 shows a comparison of the time-step bias between our previous work[73,74] and the

Table 4: DMC energy differences in kcal/mol/cell, $\Delta E_{\rm DMC} = E_{\rm DMC}(\alpha) - E_{\rm DMC}(\beta)$, between the α and β phases of p-DIB molecular crystals, evaluated for different values of $\delta\tau_{\rm DMC}$.

	T-move	$\delta\tau_{\rm DMC}$	$N_{\rm step}$	$N_{\rm pop}$	$E_{\rm DMC}(\alpha)$	$E_{\rm DMC}(\beta)$	$\Delta E_{\rm DMC}$
previous[a]	no	0.001	1.2×10^7	16,384	-148880 ± 1	-148877 ± 1	-2 ± 1
present[b]	no	0.005	6×10^4	1,280	-148871 ± 2	-148869 ± 2	-2 ± 3
present	no	0.010	3×10^4	1,280	-148863 ± 2	-148859 ± 3	-4 ± 3
present	no	0.015	3×10^4	1,280	-148860 ± 2	-148853 ± 2	-8 ± 3
present	yes	0.001	6×10^4	1,280	-148821 ± 4	-148817 ± 4	-4 ± 6
present	yes	0.002	6×10^4	1,280	-148822 ± 2	-148819 ± 2	-3 ± 3
present	yes	0.005	1.8×10^5	1,280	-148822 ± 1	-148820 ± 1	-2 ± 2
present	yes	0.008	1.2×10^5	1,280	-148825 ± 1	-148821 ± 1	-4 ± 2
present	yes	0.010	1.2×10^5	1,280	-148826 ± 1	-148822 ± 1	-4 ± 1
present	yes	0.015	1.2×10^5	1,280	-148830 ± 1	-148826 ± 1	-4 ± 1

[a] "previous" indicates the previous result in Ref.[73]
[b] "present" gives the present results.

present ones with a 1×1×1 simulation cell. We managed to find consistency between the old and new results at sufficiently small $\delta\tau_{\rm DMC}$, but the achieved error bars are not satisfactorily small. This is because we cannot keep on accumulating more statistics in the face of the population explosion when we do not use T-move. For the larger $\delta\tau_{\rm DMC} = 0.010/0.015$ (0.005) without T-move, the population explosions actually occur and then we can not exceed $N_{\rm step}$ greater than 30,000 (60,000), giving rise to the larger error bars. This is the reason for the choice of $\delta\tau_{\rm DMC} = 0.001$ and the sufficiently large population ($N_{\rm pop} = 16,384$) in our previous work[73,74] to avoid the population explosions when using a QMC implementation without T-move.[89] It is also observed in the present study that the simulations with $\delta\tau_{\rm DMC}$ larger than 0.015 are impossible due to the instability of DMC/LDA/1×1×1 with respect to population explosion.

The strong time step bias seen in Table 4 is found to be reduced considerably when we apply the T-move scheme. Figure 5 shows the time step dependence of $\Delta E_{\rm DMC}$ with T-move for DMC/LDA/1×1×1, $N_{\rm step} = 10^5$ and $N_{\rm pop} = 1,280$. We can see that the result at $\delta\tau_{\rm DMC} = 0.01$ agrees with those at smaller $\delta\tau_{\rm DMC}$. The calculations give quite stable

population control without any explosion, enabling us to try larger $1 \times 3 \times 3$ simulations and investigate the FSEs. We note that the χ^2 fitting to a linear function gives us an extrapolation, $\delta\tau_{\mathrm{DMC}} \to 0$, with $\Delta E_{\mathrm{DMC}} = -3 \pm 2$ kcal/mol/cell, giving good agreement with the previous results. Using 2,048 cores on the K computer[75] we chose N_{pop} to be $20,480$. This is due to the fact that the larger N_{pop} leads to a better load-balancing in DMC parallel computing.[56] To keep the total number of statistics, $N_{\mathrm{pop}} \times N_{\mathrm{step}}$, for both the 1×1×1 and 1×3×3 for comparison we took N_{step} to be 7×10^3. Note that we estimated the time-step bias within the 1×1×1 cell size. We could not afford several 1×3×3 simulations with different time steps within the limited resources. Then we relied on the $1 \times 1 \times 1$ result to estimate an appropriate time step for $1 \times 3 \times 3$ ($\delta\tau_{\mathrm{DMC}} = 0.01$), expecting that the time-step bias would not matter.

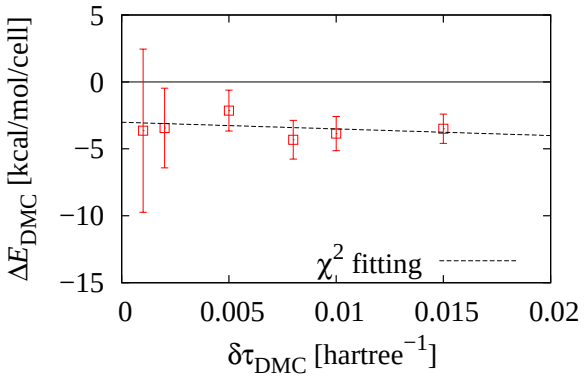

Figure 5: Plots of the DMC time step ($\delta\tau_{\mathrm{DMC}}$) versus the DMC/LDA/$1 \times 1 \times 1$ energy difference between the α and β polymorphs of p-DIB, $\Delta E_{\mathrm{DMC}} = E_{\mathrm{DMC}}(\alpha) - E_{\mathrm{DMC}}(\beta)$. The DMC simulations were performed with a 1×1×1 cell size using the T-move scheme. Energies are given in units of kcal/mol per unit cell. The χ^2 fitting (linear) is also drawn.

Concluding Remarks

We have performed, for the first time, a rigorous study of finite-size errors (FSEs) and choice of nodal surface on the prediction of polymorph stability in molecular crystals using fixed-node DMC. Our calculations are the largest which are currently feasible using the resources

of the K computer. Our results show that our previous predictions in Ref[73,74] using a small $(1 \times 1 \times 1)$ simulation cell were fortuitously accurate. Our new DMC simulations with a 1×3×3 simulation cell, using a PBE functional to generate the nodal surface, yield the same prediction for the polymorph stability, and agree with experiment. However, our observations of the finite-size effects and the choice of nodal surface provide insights into the formidable challenge of predicting such properties from first principles.

In particular, we applied the MPC and kinetic energy finite-size correction schemes to the DMC/PBE/$1 \times 3 \times 3$ calculations, where the simulation cell was approximately cubic and we accumulated statistical samples with $\sim 6.4 \times 10^5$ core-hours for each polymorph. To the best of our knowledge, this is the largest such calculation to date. However, it was found that the MPC and kinetic energy corrections to the energy difference between the polymorphs were larger than the original difference itself. The two corrections themselves significantly contribute to the total energy for each polymorph, indicating that even larger simulation cells are needed, with extrapolation to infinity. On the other hand, we show that a calculation with the next largest simulation cell, $2 \times 6 \times 6$, is unfeasible, even with hundreds of thousands of cores and the large memory capacities provided by massively-parallel conventional supercomputers. This is because the current equilibration implementations cannot be accelerated by MPI parallelization. We therefore conclude that technical advances are needed to accelerate the equilibration step if a more complete understanding of FSEs in DMC simulations of systems with large anisotropic unit cells is to be achieved.

We also found a considerable effect of finite-size errors on the trial nodal surface in the DMC/1×1×1 calculations. This may be attributed to the fact that the MPC corrections are evaluated using the DFT charge densities where the unit cell is strongly anisotropic with an aspect ratio of 3 : 1. At the DFT level, we found that there is a significant dependence of the converged values on the choice of the aspect ratio when using small cells, though extrapolations with larger cells converge to the same energy. This highlights another issue which must be carefully managed in future studies. In order to reach a decisive conclusion about the

dependence of the trial nodes on the FSE, we must at least carry out a DMC/LDA/1×3×3 calculation in addition. Unfortunately, our CPU allocation on the K computer is currently exhausted due to our other simulations, so this will need to be done in a future study.

Finally, this work illustrates the technical importance of the T-move scheme in such large-scale DMC simulations. We note that our QMC calculations would have been impossible without this technique, due to unstable population behavior and a large time-step bias.

Acknowledgments

Computations have been performed using the K computer at the RIKEN Advanced Institute for Computational Science and the computer facilities at the Research Center for Advanced Computing Infrastructure, JAIST. R.M. is grateful for financial support from KAKENHI grants (23104714, 22104011, and 25600156), and from the Tokuyama Science Foundation.

References

(1) Bernstein, J. *Polymorphism in Molecular Crystals*; Oxford University Press: New York, 2002.

(2) Moulton, B.; Zaworotko, M. J. From Molecules to Crystal Engineering: Supramolecular Isomerism and Polymorphism in Network Solids. *Chem. Rev.* **2001**, *101*, 1629–1658, PMID: 11709994.

(3) Hirata, S.; Gilliard, K.; He, X.; Li, J.; Sode, O. Ab Initio Molecular Crystal Structures, Spectra, and Phase Diagrams. *Acc. Chem. Res.* **2014**, *47*, 2721–2730, PMID: 24754304.

(4) Sharkas, K.; Toulouse, J.; Maschio, L.; Civalleri, B. Double-hybrid density-functional theory applied to molecular crystals. *J. Chem. Phys.* **2014**, *141*, 044105:1–8.

(5) Presti, D.; Pedone, A.; Menziani, M. C.; Civalleri, B.; Maschio, L. Oxalyl dihydrazide polymorphism: a periodic dispersion-corrected DFT and MP2 investigation. *Cryst. Eng. Comm.* **2014**, *16*, 102–109.

(6) Reilly, A. M.; Tkatchenko, A. Seamless and Accurate Modeling of Organic Molecular Materials. *J. Phys. Chem. Lett.* **2013**, *4*, 1028–1033.

(7) Marom, N.; DiStasio, R. A.; Atalla, V.; Levchenko, S.; Reilly, A. M.; Chelikowsky, J. R.; Leiserowitz, L.; Tkatchenko, A. Many-Body Dispersion Interactions in Molecular Crystal Polymorphism. *Angew. Chem., Int. Ed.* **2013**, *52*, 6629–6632.

(8) Wen, S.; Beran, G. J. O. Crystal Polymorphism in Oxalyl Dihydrazide: Is Empirical DFT-D Accurate Enough? *J. Chem. Theory Comput.* **2012**, *8*, 2698–2705.

(9) Wen, S.; Beran, G. J. O. Accidental Degeneracy in Crystalline Aspirin: New Insights from High-Level ab Initio Calculations. *Cryst. Growth Des.* **2012**, *12*, 2169–2172.

(10) Pedone, A.; Presti, D.; Menziani, M. C. On the ability of periodic dispersion-corrected DFT calculations to predict molecular crystal polymorphism in para-diiodobenzene. *Chem. Phys. Lett.* **2012**, *541*, 12 – 15.

(11) Bygrave, P. J.; Allan, N. L.; Manby, F. R. The embedded many-body expansion for energetics of molecular crystals. *J. Chem. Phys.* **2012**, *137*, 164102.

(12) Taylor, C. R.; Bygrave, P. J.; Hart, J. N.; Allan, N. L.; Manby, F. R. Improving density functional theory for crystal polymorph energetics. *Phys. Chem. Chem. Phys.* **2012**, *14*, 7739–7743.

(13) Wen, S.; Nanda, K.; Huang, Y.; Beran, G. J. O. Practical quantum mechanics-based fragment methods for predicting molecular crystal properties. *Phys. Chem. Chem. Phys.* **2012**, *14*, 7578–7590.

(14) Nanda, K. D.; Beran, G. J. O. Prediction of organic molecular crystal geometries from MP2-level fragment quantum mechanical/molecular mechanical calculations. *J. Chem. Phys.* **2012**, *137*, 174106.

(15) Sancho-García, J. C.; Olivier, Y. Reliable DFT-based estimates of cohesive energies of organic solids: The anthracene crystal. *J. Chem. Phys.* **2012**, *137*, 194311.

(16) Wen, S.; Beran, G. J. O. Accurate Molecular Crystal Lattice Energies from a Fragment QM/MM Approach with On-the-Fly Ab Initio Force Field Parametrization. *J. Chem. Theory Comput.* **2011**, *7*, 3733–3742.

(17) Habgood, M.; Price, S. L.; Portalone, G.; Irrera, S. Testing a Variety of Electronic-Structure-Based Methods for the Relative Energies of 5-Formyluracil Crystals. *J. Chem. Theory Comput.* **2011**, *7*, 2685–2688.

(18) Jacobsen, H. A Failure of DFT Is Not Necessarily a DFT Failure-Performance Dependencies on Model System Choices. *J. Chem. Theory Comput.* **2011**, *7*, 3019–3025.

(19) Taylor, D. E.; Rob, F.; Rice, B. M.; Podeszwa, R.; Szalewicz, K. A molecular dynamics study of 1,1-diamino-2,2-dinitroethylene (FOX-7) crystal using a symmetry adapted perturbation theory-based intermolecular force field. *Phys. Chem. Chem. Phys.* **2011**, *13*, 16629–16636.

(20) Beran, G. J. O.; Nanda, K. Predicting Organic Crystal Lattice Energies with Chemical Accuracy. *J. Phys. Chem. Lett.* **2010**, *1*, 3480–3487.

(21) Moellmann, J.; Grimme, S. Importance of London dispersion effects for the packing of molecular crystals: a case study for intramolecular stacking in a bis-thiophene derivative. *Phys. Chem. Chem. Phys.* **2010**, *12*, 8500–8504.

(22) de-la Roza, A. O.; Johnson, E. R. A benchmark for non-covalent interactions in solids. *J. Chem. Phys.* **2012**, *137*, 054103.

(23) Hirata, S. Bridging quantum chemistry and solid-state physics. *Mol. Phys.* **2010**, *108*, 3113–3124.

(24) Hirata, S. Quantum chemistry of macromolecules and solids. *Phys. Chem. Chem. Phys.* **2009**, *11*, 8397–8412.

(25) Sode, O.; Keçeli, M.; Hirata, S.; Yagi, K. Coupled-cluster and many-body perturbation study of energies, structures, and phonon dispersions of solid hydrogen fluoride. *Int. J. Quantum Chem.* **2009**, *109*, 1928–1939.

(26) Neumann, M. A.; Perrin, M.-A. Can crystal structure prediction guide experimentalists to a new polymorph of paracetamol? *Cryst. Eng. Comm.* **2009**, *11*, 2475–2479.

(27) Price, S. L. Computational prediction of organic crystal structures and polymorphism. *Int. Rev. Phys. Chem.* **2008**, *27*, 541–568.

(28) Woodley, S. M.; Catlow, R. Crystal structure prediction from first principles. *Nat. Mater.* **2008**, *7*, 937–946.

(29) Podeszwa, R.; Rice, B. M.; Szalewicz, K. Predicting Structure of Molecular Crystals from First Principles. *Phys. Rev. Lett.* **2008**, *101*, 115503.

(30) Neumann, M.; Leusen, F.; Kendrick, J. A Major Advance in Crystal Structure Prediction. *Angew. Chem., Int. Ed.* **2008**, *47*, 2427–2430.

(31) Brillante, A.; Della Valle, R. G.; Farina, L.; Venuti, E.; Cavazzoni, C.; Emerson, A. P. J.; Syassen, K. High-Pressure Dissociation of Crystalline para-Diiodobenzene: Experiments and Car-Parrinello Calculations. *J. Am. Chem. Soc.* **2005**, *127*, 3038–3043, PMID: 15740142.

(32) Price, S. L. The computational prediction of pharmaceutical crystal structures and polymorphism. *Adv. Drug Delivery Rev.* **2004**, *56*, 301 – 319, Pharmaceutical solid polymorphism in drug development and regulation.

(33) Hohenberg, P.; Kohn, W. Inhomogeneous Electron Gas. *Phys. Rev.* **1964**, *136*, B864–B871.

(34) Kohn, W.; Sham, L. Self-Consistent Equations Including Exchange and Correlation Effects. *Phys. Rev.* **1965**, *140*, A1133–A1138.

(35) Cohen, A. J.; Mori-Sánchez, P.; Yang, W. Challenges for Density Functional Theory. *Chem. Rev.* **2012**, *112*, 289–320.

(36) Grimme, S. Density functional theory with London dispersion corrections. *WIRs: Comput. Mol. Sci.* **2011**, *1*, 211–228.

(37) Ehrlich, S.; Moellmann, J.; Grimme, S. Dispersion-Corrected Density Functional Theory for Aromatic Interactions in Complex Systems. *Acc. Chem. Res.* **2013**, *46*, 916–926.

(38) Zhao, Y.; Schultz, N. E.; Truhlar, D. G. Exchange-correlation functional with broad accuracy for metallic and nonmetallic compounds, kinetics, and noncovalent interactions. *J. Chem. Phys.* **2005**, *123*, 161103.

(39) Peverati, R.; Truhlar, D. G. Improving the Accuracy of Hybrid Meta-GGA Density Functionals by Range Separation. *J. Phys. Chem. Lett.* **2011**, *2*, 2810–2817.

(40) Yanai, T.; Tew, D. P.; Handy, N. C. A new hybrid exchangecorrelation functional using the Coulomb-attenuating method (CAM-B3LYP). *Chem. Phys. Lett.* **2004**, *393*, 51 – 57.

(41) Heßelmann, A.; Jansen, G.; Schütz, M. Density-functional theory-symmetry-adapted intermolecular perturbation theory with density fitting: A new efficient method to study intermolecular interaction energies. *J. Chem. Phys.* **2005**, *122*, 014103.

(42) Szalewicz, K. Symmetry-adapted perturbation theory of intermolecular forces. *WIRs: Comput. Mol. Sci.* **2012**, *2*, 254–272.

(43) Dion, M.; Rydberg, H.; Schröder, E.; Langreth, D. C.; Lundqvist, B. I. Van der Waals Density Functional for General Geometries. *Phys. Rev. Lett.* **2004**, *92*, 246401.

(44) Tkatchenko, A.; Scheffler, M. Accurate Molecular Van Der Waals Interactions from Ground-State Electron Density and Free-Atom Reference Data. *Phys. Rev. Lett.* **2009**, *102*, 073005.

(45) Tkatchenko, A.; DiStasio, R. A.; Car, R.; Scheffler, M. Accurate and Efficient Method for Many-Body van der Waals Interactions. *Phys. Rev. Lett.* **2012**, *108*, 236402.

(46) Helgaker, T.; Jørgensen, P.; Olsen, P. *Molecular Electronic-Structure Theory*; Wiley: Chichester, U.K., 2000.

(47) Hongo, K.; Cuong, N. T.; Maezono, R. The Importance of Electron Correlation on Stacking Interaction of Adenine-Thymine Base-Pair Step in B-DNA: A Quantum Monte Carlo Study. *J. Chem. Theory Comput.* **2013**, *9*, 1081–1086.

(48) Needs, R. J.; Towler, M. D.; Drummond, N. D.; Ríos, P. L. Continuum variational and diffusion quantum Monte Carlo calculations. *J. Phys. Condens. Matter* **2010**, *22*, 023201.

(49) Austin, B. M.; Zubarev, D. Y.; Lester, W. A. Quantum Monte Carlo and Related Approaches. *Chem. Rev.* **2012**, *112*, 263–288.

(50) Lüchow, A. Quantum Monte Carlo methods. *WIRs: Comput. Mol. Sci.* **2011**, *1*, 388–402.

(51) Grossman, J. C. Benchmark quantum Monte Carlo calculations. *J. Chem. Phys.* **2002**, *117*, 1434–1440.

(52) Korth, M.; Luchow, A.; Grimme, S. Toward the Exact Solution of the Electronic Schrodinger Equation for Noncovalent Molecular Interactions: Worldwide Distributed

Quantum Monte Carlo Calculations. *J. Phys. Chem. A* **2008**, *112*, 2104–2109, PMID: 18201073.

(53) Horváthová, L.; Dubecký, M.; Mitas, L.; Štich, I. Quantum Monte Carlo Study of π-Bonded Transition Metal Organometallics: Neutral and Cationic VanadiumBenzene and CobaltBenzene Half Sandwiches. *J. Chem. Theory Comput.* **2013**, *9*, 390–400.

(54) Dubecký, M.; Jurečka, P.; Derian, R.; Hobza, P.; Otyepka, M.; Mitas, L. Quantum Monte Carlo Methods Describe Noncovalent Interactions with Subchemical Accuracy. *J. Chem. Theory Comput.* **2013**, *9*, 4287–4292.

(55) Sudheer, C.; Krishnan, S.; Srinivasan, A.; Kent, P. Dynamic load balancing for petascale quantum Monte Carlo applications: The Alias method. *Comput. Phys. Commun.* **2013**, *184*, 284 – 292.

(56) Gillan, M. J.; Towler, M. D.; Alè, D. *Petascale computing opens new vistas for quantum Monte Carlo*; Psi-k Highlight of the Month, 2011.

(57) Drummond, N. D.; Needs, R. J.; Sorouri, A.; Foulkes, W. M. C. Finite-size errors in continuum quantum Monte Carlo calculations. *Phys. Rev. B* **2008**, *78*, 125106.

(58) Lin, C.; Zong, F. H.; Ceperley, D. M. Twist-averaged boundary conditions in continuum quantum Monte Carlo algorithms. *Phys. Rev. E* **2001**, *64*, 016702.

(59) Rajagopal, G.; Needs, R. J.; Kenny, S.; Foulkes, W. M. C.; James, A. Quantum Monte Carlo Calculations for Solids Using Special k Points Methods. *Phys. Rev. Lett.* **1994**, *73*, 1959–1962.

(60) Rajagopal, G.; Needs, R. J.; James, A.; Kenny, S. D.; Foulkes, W. M. C. Variational and diffusion quantum Monte Carlo calculations at nonzero wave vectors: Theory and application to diamond-structure germanium. *Phys. Rev. B* **1995**, *51*, 10591–10600.

(61) Fraser, L. M.; Foulkes, W. M. C.; Rajagopal, G.; Needs, R. J.; Kenny, S. D.; Williamson, A. J. Finite-size effects and Coulomb interactions in quantum Monte Carlo calculations for homogeneous systems with periodic boundary conditions. *Phys. Rev. B* **1996**, *53*, 1814–1832.

(62) Williamson, A. J.; Rajagopal, G.; Needs, R. J.; Fraser, L. M.; Foulkes, W. M. C.; Wang, Y.; Chou, M.-Y. Elimination of Coulomb finite-size effects in quantum many-body simulations. *Phys. Rev. B* **1997**, *55*, R4851–R4854.

(63) Chiesa, S.; Ceperley, D. M.; Martin, R. M.; Holzmann, M. Finite-Size Error in Many-Body Simulations with Long-Range Interactions. *Phys. Rev. Lett.* **2006**, *97*, 076404.

(64) Kwee, H.; Zhang, S.; Krakauer, H. Finite-Size Correction in Many-Body Electronic Structure Calculations. *Phys. Rev. Lett.* **2008**, *100*, 126404.

(65) Ma, F.; Zhang, S.; Krakauer, H. Finite-size correction in many-body electronic structure calculations of magnetic systems. *Phys. Rev. B* **2011**, *84*, 155130.

(66) Kolorenč, J.; Mitas, L. Applications of quantum Monte Carlo methods in condensed systems. *Rep. Prog. Phys.* **2011**, *74*, 026502.

(67) Hood, R. Q.; Kent, P. R. C.; Reboredo, F. A. Diffusion quantum Monte Carlo study of the equation of state and point defects in aluminum. *Phys. Rev. B* **2012**, *85*, 134109.

(68) Ouma, C. N. M.; Mapelu, M. Z.; Makau, N. W.; Amolo, G. O.; Maezono, R. Quantum Monte Carlo study of pressure-induced $B3-B1$ phase transition in GaAs. *Phys. Rev. B* **2012**, *86*, 104115.

(69) Ertekin, E.; Wagner, L. K.; Grossman, J. C. Point-defect optical transitions and thermal ionization energies from quantum Monte Carlo methods: Application to the F-center defect in MgO. *Phys. Rev. B* **2013**, *87*, 155210.

(70) Shulenburger, L.; Mattsson, T. R. Quantum Monte Carlo applied to solids. *Phys. Rev. B* **2013**, *88*, 245117.

(71) Santra, B.; Klimeš, J. c. v.; Alfè, D.; Tkatchenko, A.; Slater, B.; Michaelides, A.; Car, R.; Scheffler, M. Hydrogen Bonds and van der Waals Forces in Ice at Ambient and High Pressures. *Phys. Rev. Lett.* **2011**, *107*, 185701.

(72) Azadi, S.; Foulkes, W. M. C.; Kühne, T. D. Quantum Monte Carlo study of high pressure solid molecular hydrogen. *New J. Phys.* **2013**, *15*, 113005.

(73) Hongo, K.; Watson, M. A.; Sánchez-Carrera, R. S.; Iitaka, T.; Aspuru-Guzik, A. Failure of Conventional Density Functionals for the Prediction of Molecular Crystal Polymorphism: A Quantum Monte Carlo Study. *J. Phys. Chem. Lett.* **2010**, *1*, 1789–1794.

(74) Watson, M. A.; Hongo, K.; Iitaka, T.; Aspuru-Guzik, A. *Advances in Quantum Monte Carlo*; Chapter 10, pp 101–117.

(75) K computer at RIKEN, Japan. `http://www.riken.go.jp/en/research/environment/kcomputer/`, Accessed: 2014-04-28.

(76) Aliev, A. E.; Harris, K. D. M.; Alcobea, X.; Estop, E. Dynamic properties of p-diiodobenzene investigated by solid-state 2H and 13C nuclear magnetic resonance spectroscopy. *J. Chem. Soc., Faraday Trans.* **1993**, *89*, 3797–3800.

(77) Alcobé, X.; Estop, E.; Aliev, A. E.; Harris, K. D.; Rodrguez-Carvajal, J.; Rius, J. Temperature-Dependent Structural Properties of p-Diiodobenzene: Neutron Diffraction and High-Resolution Solid State ^{13}C NMR Investigations. *J. Solid State Chem.* **1994**, *110*, 20 – 27.

(78) The Cambridge Structural Database. `http://www.ccdc.cam.ac.uk/`, Accessed: 2014-10-27.

(79) Monkhorst, H. J.; Pack, J. D. Special points for Brillouin-zone integrations. *Phys. Rev. B* **1976**, *13*, 5188–5192.

(80) Perdew, J. P.; Zunger, A. Self-interaction correction to density-functional approximations for many-electron systems. *Phys. Rev. B* **1981**, *23*, 5048–5079.

(81) Perdew, J. P.; Burke, K.; Ernzerhof, M. Generalized Gradient Approximation Made Simple. *Phys. Rev. Lett.* **1996**, *77*, 3865–3868.

(82) Lee, C.; Yang, W.; Parr, R. G. Development of the Colle-Salvetti correlation-energy formula into a functional of the electron density. *Phys. Rev. B* **1988**, *37*, 785–789.

(83) Becke, A. D. Density-functional thermochemistry. III. The role of exact exchange. *J. Chem. Phys.* **1993**, *98*, 5648–5652.

(84) Stephens, P. J.; Devlin, F. J.; Chabalowski, C. F.; Frisch, M. J. Ab Initio Calculation of Vibrational Absorption and Circular Dichroism Spectra Using Density Functional Force Fields. *J. Phys. Chem.* **1994**, *98*, 11623–11627.

(85) Giannozzi, P. et al. QUANTUM ESPRESSO: a modular and open-source software project for quantum simulations of materials. *J. Phys. Condens. Matter* **2009**, *21*, 395502 (19pp).

(86) Trail, J. R.; Needs, R. J. Smooth relativistic Hartree–Fock pseudopotentials for H to Ba and Lu to Hg. *J. Chem. Phys.* **2005**, *122*, 174109.

(87) Trail, J. R.; Needs, R. J. Norm-conserving Hartree–Fock pseudopotentials and their asymptotic behavior. *J. Chem. Phys.* **2005**, *122*, 014112.

(88) CASINO pseudopotential library. `http://vallico.net/casinoqmc/pplib/`, Accessed: 2014-10-27.

(89) QMCPACK. `https://code.google.com/p/qmcpack/`, Accessed: 2014-10-27.

(90) Perdew, J. P.; Wang, Y. Accurate and simple analytic representation of the electron-gas correlation energy. *Phys. Rev. B* **1992**, *45*, 13244–13249.

(91) Gonze, X. A brief introduction to the ABINIT software package. *Z. Kristallogr.* **2005**, *220*, 558–562.

(92) Gonze, X.; Amadon, B.; Anglade, P.-M.; Beuken, J.-M.; Bottin, F.; Boulanger, P.; Bruneval, F.; Caliste, D.; Caracas, R.; Côté, M. ABINIT: First-principles approach to material and nanosystem properties. *Comput. Phys. Commun.* **2009**, *180*, 2582–2615.

(93) Casula, M. Beyond the locality approximation in the standard diffusion Monte Carlo method. *Phys. Rev. B* **2006**, *74*, 161102.

(94) Alfè, D.; Gillan, M. J. Efficient localized basis set for quantum Monte Carlo calculations on condensed matter. *Phys. Rev. B* **2004**, *70*, 161101.

(95) Jastrow, R. Many-Body Problem with Strong Forces. *Phys. Rev.* **1955**, *98*, 1479–1484.

(96) Drummond, N. D.; Towler, M. D.; Needs, R. J. Jastrow correlation factor for atoms, molecules, and solids. *Phys. Rev. B* **2004**, *70*, 235119.

(97) Kato, T. On the eigenfunctions of many-particle systems in quantum mechanics. *Commun. Pur. App. Math.* **1957**, *10*, 151–177.

(98) Umrigar, C. J.; Filippi, C. Energy and Variance Optimization of Many-Body Wave Functions. *Phys. Rev. Lett.* **2005**, *94*, 150201.

(99) Drummond, N. D.; Needs, R. J. Variance-minimization scheme for optimizing Jastrow factors. *Phys. Rev. B* **2005**, *72*, 085124.

(100) Ewald, P. P. Die Berechnung optischer und elektrostatischer Gitterpotentiale. *Ann. Phys.* **1921**, *369*, 253–287.

(101) Allen, M.; Tildesley, D. *Computer Simulation of Liquids*; Oxford University Press: New York, 1990.

(102) Umrigar, C. J.; Nightingale, M. P.; Runge, K. J. A diffusion Monte Carlo algorithm with very small time-step errors. *J. Chem. Phys.* **1993**, *99*, 2865–2890.

(103) Hasegawa, M.; Nishidate, K. Semiempirical approach to the energetics of interlayer binding in graphite. *Phys. Rev. B* **2004**, *70*, 205431.

(104) Tkatchenko, A.; von Lilienfeld, O. A. Popular Kohn-Sham density functionals strongly overestimate many-body interactions in van der Waals systems. *Phys. Rev. B* **2008**, *78*, 045116.

(105) Maezono, R.; Towler, M. D. private communication, 2013.

(106) Umrigar, C. J.; Nightingale, M. P.; Runge, K. J. A diffusion Monte Carlo algorithm with very small time-step errors. *J. Chem. Phys.* **1993**, *99*, 2865–2890.

(107) Uejima, Y.; Terashima, T.; Maezono, R. Acceleration of a QM/MM-QMC simulation using GPU. *J. Comput. Chem.* **2011**, *32*, 2264–2272.

(108) Uejima, Y.; Maezono, R. GPGPU for orbital function evaluation with a new updating scheme. *J. Comput. Chem.* **2013**, *34*, 83–94.

(109) Gothandaraman, A.; Peterson, G. D.; Warren, G.; Hinde, R. J.; Harrison, R. J. FPGA acceleration of a quantum Monte Carlo application. *Parallel Comput.* **2008**, *34*, 278 – 291, Reconfigurable Systems Summer Institute 2007.

(110) Weber, R.; Gothandaraman, A.; Hinde, R. J.; Peterson, G. D. Comparing Hardware Accelerators in Scientific Applications: A Case Study. *IEEE Trans. Parallel Distrib. Syst.* **2011**, *22*, 58–68.

(111) Reynolds, P. J.; Ceperley, D. M.; Alder, B. J.; Lester, W. A. Fixed-node quantum Monte Carlo for molecules. *J. Chem. Phys.* **1982**, *77*, 5593–5603.

(112) Mitáš, L.; Shirley, E. L.; Ceperley, D. M. Nonlocal pseudopotentials and diffusion Monte Carlo. *J. Chem. Phys.* **1991**, *95*, 3467–3475.

Graphical TOC Entry

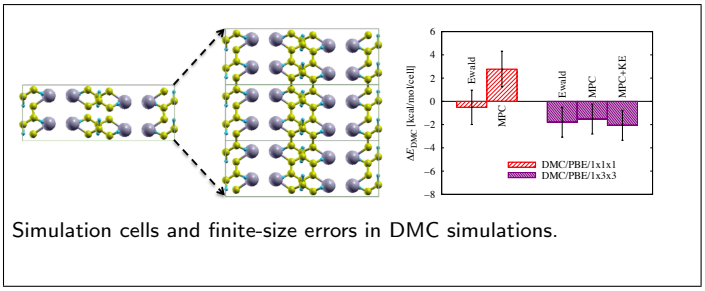

Simulation cells and finite-size errors in DMC simulations.